# Magnetotransport through graphene spin valves

Kai-He Ding,[1] Zhen-Gang Zhu,[2] and Jamal Berakdar[2]
[1]*Department of Physics and Electronic Science, Changsha University of Science and Technology, Changsha 410076, China*
[2]*Institut für Physik, Martin-Luther-Universität Halle-Wittenberg, Nanotechnikum-Weinberg, Heinrich-Damerow-Strasse 4 D-06120 Halle (Saale), Germany*
(Received 22 August 2008; published 9 January 2009)

We present a theoretical study on the spin-dependent transport through a spin valve consisting of graphene sandwiched between two magnetic leads with an arbitrary orientation of the lead magnetization. No gate voltage is applied. Using Keldysh's nonequilibrium Green's function method we show that, in absence of external magnetic fields, the current-voltage curves are nonlinear. Around zero bias the differential conductance versus bias voltage possesses a strong dip. The zero-bias anomaly in the tunnel magnetoresistance (TMR) is affected strongly by the leads' spin polarization. Depending on the value of the bias-voltage TMR exhibits a behavior ranging from an insulating to a metallic type. In presence of a static external magnetic field the differential conductance and TMR as a function of the bias voltage and the strength of the magnetic field show periodic oscillations due to Landau-level crossings. We also inspect the effects of the temperature and the polarization degrees on the differential conductance and TMR.

DOI: 10.1103/PhysRevB.79.045405 PACS number(s): 81.05.Uw, 75.47.−m, 85.75.−d

## I. INTRODUCTION

Recent advances in nanoscience techniques opened the way for the creation and the investigation of the two-dimensional carbon, also called graphene.[1–4] This system is a monolayer of carbon atoms packed densely into a honeycomb lattice, and can be viewed as the basic building block for many carbon-based materials with other dimensionalities, including fullerene, nanotube, graphite, etc. Its low energy band structure consists of two inequivalent pairs of cones with apices located at the Brillouin-zone corners.[5] In these cones, the energy-dispersion relation is linear, and the dynamics of the charge carriers is governed by a massless Dirac-type equation. The form of the electronic band structure is expected to lead to a number of unusual electronic properties in graphene such as the anomalous quantized Hall effect, the absence of the weak localization, and the existence of the minimal conductivity.[6] Graphene is also an interesting candidate for transport applications, in particular for spintronics: the mobility is remarkably high and the carrier density is controllable by a gate voltage. In addition, spin-dependent interactions can be exploited for the control of the magnetoconductance.[7–12] Motivated by these facts, the spin-dependent properties of graphene are in the focus of current research; e.g., Hill *et al.*[13] fabricated graphene spin-valve device and observed a 10% change in the resistance as the electrodes switch from a parallel to an antiparallel state. Recent experiments on spin injection in a single layer graphene show a rather long spin-flip length ($\approx 1$ $\mu$m) at room temperature.[14] Spin injection into a graphene thin film has been successfully demonstrated by using nonlocal magnetoresistance measurements.[14–16] Wang *et al.*[17] measured the magnetoresistance of mesoscopic graphite spin-valve devices and observed a cusplike feature of the magnetoresistance versus the applied bias and pointed out the importance of spin-dependent interfacial resistance for spin injection.

In this work we investigate theoretically the spin-dependent transport through a graphene spin-valve device with ferromagnetic leads having arbitrary spin-polarization directions. No gate voltage is applied. Utilizing Keldysh's nonequilibrium Green's function method[18] we calculate the density of states (DOS) and the electrical current in the ferromagnet-graphene-ferromagnet (FM-G-FM) coupled system. The differential conductance and the tunnel magnetoresistance are also calculated without and with a static external magnetic field at finite temperatures. We found that at zero magnetic fields, the current-voltage curves in this spintronic structure show a nonlinear characteristic; the differential conductance as a function of the applied voltage exhibits a strong dip near zero bias. The behavior of the zero-bias anomaly in TMR is governed by the leads' spin polarization. With increasing the temperature, the dip in the differential conductance and the cusp in TMR near zero bias diminish. When both the spin-polarization degrees and the relative angles of the two ferromagnetic moments are large, the differential conductance is small due to the influence of both the DOS in graphene and the conventional spin-valve effect. In the presence of a static magnetic field, the differential conductance and TMR show periodic oscillations due to a resonant transport though the Landau levels when the bias-voltage values are appropriate. At zero-bias voltage, the differential conductance versus the temperature shows a behavior different from the field-free case. We attribute this fact to the breaking of the insulator-type properties of graphene at finite magnetic fields.

The rest of this paper is organized as follows. In Sec. II, we introduce the model and derive the current formula in the absence of the magnetic field. In Sec. III, the magnetotransport properties of this system are computed at finite external magnetic fields. In Sec. IV, the corresponding numerical results are given. Finally, a summary is presented.

## II. THEORETICAL MODEL

We consider a spin-valve device consisting of a graphene layer contacted to ferromagnetic electrodes, as shown in Fig.

 

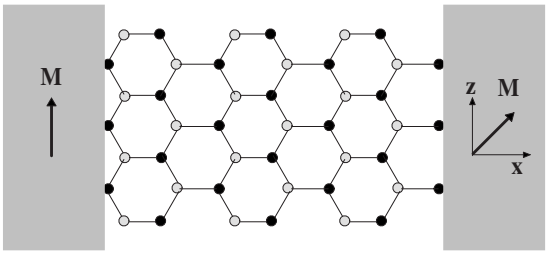


FIG. 1. Schematic illustration of the system considered in this work. The graphene is connected to two magnetic leads by the tunneling barriers. The moments of the leads are aligned by a relative angle $\theta$, and the coupling matrix between $\alpha$ ($\alpha$=$L$,$R$) electrode and graphene is $T_{k\alpha}$.

1. The moment $\mathbf{M}_L$ of the left electrode is assumed to define the $z$ direction, while the moment $\mathbf{M}_R$ of the right electrode deviates from the $z$ direction by a relative angle $\theta$. A bias voltage $V$ is applied between the left and the right electrodes. The electrical current flows in the $x$ direction. The left and the right electrodes can be described by Hamiltonians,

$$H_L = \sum_{\mathbf{k},\sigma} \varepsilon_{\mathbf{k}L\sigma} c^\dagger_{\mathbf{k}L\sigma} c_{\mathbf{k}L\sigma}, \tag{1}$$

$$H_R = \sum_{\mathbf{k},\sigma} [\varepsilon_R(\mathbf{k}) - \sigma \mathbf{M}_R \cos\theta] c^\dagger_{\mathbf{k}R\sigma} c_{\mathbf{k}R\sigma} - \mathbf{M}_R \sin\theta c^\dagger_{\mathbf{k}R\sigma} c_{\mathbf{k}R\bar{\sigma}}, \tag{2}$$

where $\varepsilon_{\mathbf{k}\alpha\sigma}$ is the single electron energy associated with the momentum $\mathbf{k}$, the spin $\sigma$ and the $\alpha$ electrode. $c^\dagger_{\mathbf{k}\alpha\sigma}(c_{\mathbf{k}\alpha\sigma})$ creates (annihilates) an electron with the energy $\varepsilon_{\mathbf{k}\alpha\sigma}$.

The tight-binding Hamiltonian of the electrons in graphene is given by

$$H_G = -t \sum_{\langle i,j\rangle,\sigma} (a^\dagger_{i,\sigma} b_{j,\sigma} + \text{H.c.}), \tag{3}$$

where $a^\dagger_{i,\sigma}(a_{i,\sigma})$ creates (annihilates) an electron with the spin $\sigma$ on the position $\mathbf{R}_i$ of the sublattice $A$, $b^\dagger_{i,\sigma}(b_{i,\sigma})$ creates (annihilates) an electron with the spin $\sigma$ on the position $\mathbf{R}_i$ on the sublattice $B$, and $t$ is the nearest-neighbor ($\langle i,j\rangle$) hopping energy. In the momentum space the Hamiltonian $H_G$ is rewritten as

$$H_G = \sum_{\mathbf{q},\sigma} [\phi(\mathbf{q}) a^\dagger_{\mathbf{q}\sigma} b_{\mathbf{q}\sigma} + \phi(\mathbf{q})^* b^\dagger_{\mathbf{q}\sigma} a_{\mathbf{q}\sigma}], \tag{4}$$

where

$$\phi(\mathbf{q}) = -t \sum_{i=1}^{3} e^{i\mathbf{q}\cdot\delta_i} \text{ with } \delta_1 = \frac{a}{2}(1,\sqrt{3},0),$$

$$\delta_2 = \frac{a}{2}(1,-\sqrt{3},0), \quad \delta_3 = a(1,0,0).$$

Here $a$ is the lattice spacing. Diagonalizing Hamiltonian (4) one finds

$$E_\pm(\mathbf{k}) = \pm t|\phi(\mathbf{k})|,$$

which can be linearized around the $\mathbf{K}$ points of the Brillouin zone leading to the dispersion

$$E_\pm(\mathbf{k}) = \pm v_F|\mathbf{k}|, \tag{5}$$

where $v_F = 3ta/2$ is the Fermi velocity of electron [$t \sim 2.3$ eV (Ref. 19)]. The coupling between the electrodes and graphene is modeled by

$$H_T = \frac{1}{\sqrt{N}} \sum_{\mathbf{kq}\alpha\sigma} [T_{\mathbf{k}\alpha\mathbf{q}} c^\dagger_{\mathbf{k}\alpha\sigma} a_{\mathbf{q}\sigma} + \text{H.c.}], \quad \alpha = L,R. \tag{6}$$

$T_{\mathbf{k}\alpha\mathbf{q}}$ is the coupling matrix between the $\alpha$ electrode and the graphene; $N$ is the number of sites on the sublattice $A$.

The electrical current from the left electrode to the graphene sheet is obtained from the time evolution of the occupation number operator of the left electrode, i.e.,

$$I = e\langle \dot{\hat{\mathcal{N}}}_L \rangle = \frac{ie}{\hbar} \langle [H, \hat{\mathcal{N}}_L] \rangle, \quad \hat{\mathcal{N}}_L = \sum_{\mathbf{k}\sigma} c^\dagger_{\mathbf{k}L\sigma} c_{\mathbf{k}L\sigma}. \tag{7}$$

Using the nonequilibrium Green's function method, Eq. (7) can be further expressed as

$$I = -\frac{ie}{\hbar N} \int \frac{d\varepsilon}{2\pi} \text{Tr} \sum_{\mathbf{qq}'} \{[G^r_{\mathbf{q}a,\mathbf{q}'a}(\varepsilon) - G^a_{\mathbf{q}a,\mathbf{q}'a}(\varepsilon)] f_L(\varepsilon) + G^<_{\mathbf{q}a,\mathbf{q}'a}(\varepsilon)\} \Gamma_{L\mathbf{q}'\mathbf{q}}(\varepsilon), \tag{8}$$

where Tr means the trace in the spin space and $f_\alpha(\varepsilon)$ is the Fermi distribution function at the energy $\varepsilon$.

$$G^{\sigma\sigma',<}_{\mathbf{q}a,\mathbf{q}'a}(t-t') = i\langle a^\dagger_{q'\sigma'}(t') a_{q\sigma}(t) \rangle$$

is the matrix expression for the lesser Green's function. $G^r_{\mathbf{q}a,\mathbf{q}'a}(\varepsilon)$ and $G^a_{\mathbf{q}a,\mathbf{q}'a}(\varepsilon)$ are $2\times2$ matrices in the spin space in the sublattice $A$ describing, respectively, the retarded and the advanced Green's function. The linewidth matrix $\Gamma_{\alpha\mathbf{qq}'}$ is given by

$$\Gamma_{\alpha\mathbf{qq}'}(\varepsilon) = \begin{pmatrix} \Gamma^\uparrow_{\alpha\mathbf{qq}'} & 0 \\ 0 & \Gamma^\downarrow_{\alpha\mathbf{qq}'} \end{pmatrix}, \tag{9}$$

$$\text{and } \Gamma^\sigma_{\alpha\mathbf{qq}'}(\varepsilon) = 2\pi \sum_{\mathbf{k}} T^*_{\mathbf{k}\alpha\mathbf{q}} T_{\mathbf{k}\alpha\mathbf{q}'} \delta(\varepsilon - \varepsilon_{\mathbf{k}\alpha\sigma}),$$

where $T_{\mathbf{k}L\mathbf{q}}$ stands for the coupling of graphene to the electrodes. To evaluate $I$ from Eq. (8) the retarded Green's function $G^r_{\mathbf{q}a,\mathbf{q}'a}(\varepsilon)$ needs to be calculated. Here we consider electrons near the Fermi level which contribute predominantly to tunneling. In this case one may assume the coupling matrix $T_{\mathbf{k}L\mathbf{q}}$ to be independent of $\mathbf{q}$ and set $\Gamma^\sigma_{\alpha\mathbf{qq}'} = \Gamma^\sigma_\alpha$. Standard Green's function technique[18] delivers,

$$G^r_{qa,q'a}(\varepsilon) = \delta_{qq'} g^r_{qa,qa}(\varepsilon) + g^r_{qa,qa}(\varepsilon) T(\varepsilon) g^r_{q'a,q'a}(\varepsilon). \tag{10}$$

In the above expressions we introduced

$$g^{r,a}_{qa,qa}(\varepsilon) = \frac{\varepsilon}{(\varepsilon \pm i\eta)^2 - |\phi(q)|^2},$$

$$\text{and } T(\varepsilon) = \frac{\Sigma^r(\varepsilon)}{1 - \bar{g}^r_{aa}(\varepsilon)\Sigma^r(\varepsilon)},$$

where

$$\bar{g}^{r,a}_{aa}(\varepsilon) = \frac{1}{N}\sum_{\mathbf{q}} g^{r,a}_{\mathbf{q}a,\mathbf{q}a}(\varepsilon),$$

$$\text{and } \Sigma^{r,a}(\varepsilon) = \mp \frac{i}{2}[\Gamma_L(\varepsilon) + R\Gamma_R(\varepsilon)R^\dagger]$$

with

$$R = \begin{pmatrix} \cos\frac{\theta}{2} & -\sin\frac{\theta}{2} \\ \sin\frac{\theta}{2} & \cos\frac{\theta}{2} \end{pmatrix}.$$

In Eq. (8), $G^<_{\mathbf{q}a,\mathbf{q}'a}(\varepsilon)$ can be derived by applying Keldysh equation

$$G^<_{\mathbf{q}a,\mathbf{q}'a}(\varepsilon) = G^r_{\mathbf{q}a,\mathbf{q}'a}(\varepsilon)\Sigma^<(\varepsilon)G^a_{\mathbf{q}a,\mathbf{q}'a}(\varepsilon)$$

with

$$\Sigma^<(\varepsilon) = i[f_L(\varepsilon)\Gamma_L(\varepsilon) + f_R(\varepsilon)R\Gamma_R(\varepsilon)R^\dagger].$$

Substituting the expressions of the graphene Green's functions in Eq. (8), and after a straightforward calculation we obtain the tunneling current as

$$I = \frac{e}{\hbar}\int \frac{d\varepsilon}{2\pi}\mathrm{Tr}\{[\mathcal{G}^r_a(\varepsilon)(R\Gamma_R(\varepsilon)R^\dagger)]\mathcal{G}^a_a(\varepsilon)\Gamma_L(\varepsilon)\}[f_R(\varepsilon) - f_L(\varepsilon)], \tag{11}$$

where

$$\mathcal{G}^{r,a}_a(\varepsilon) = \sum_{q'}\sum_{q} G^{r,a}_{qa,q'a}(\varepsilon) = \frac{\bar{g}^{r,a}_{aa}(\varepsilon)}{1 - \bar{g}^{r,a}_{aa}(\varepsilon)\Sigma^{r,a}(\varepsilon)}. \tag{12}$$

Introducing a cutoff $k_c$ leads to

$$\bar{g}^{r,a}_{aa}(\varepsilon) = -F_0(\varepsilon) \mp i\pi\rho_0(\varepsilon), \tag{13}$$

where

$$F_0(\varepsilon) = \frac{\varepsilon}{D^2}\ln\frac{|\varepsilon^2 - D^2|}{\varepsilon^2}, \quad \rho_0(\varepsilon) = \frac{|\varepsilon|}{D^2}\theta(D - |\varepsilon|). \tag{14}$$

$D = v_F k_c$ stands for a high-energy cutoff of the graphene bandwidth. Invoking the Debye's prescription, we choose $k_c$ such that the total number of states in the Brillouin zone is conserved after the linearization of the spectrum around the **K** point. Hence, Eq. (13) is accurate for $\varepsilon \ll D$, i.e., $\varepsilon$ has to be in the region where the linearization of the spectrum is justifiable which is roughly estimated[20] to be (−1.6 eV, 1.6 eV). In Eq. (12) we assumed a symmetrical voltage drop as $\mu_{L,R} = E_F \pm \frac{1}{2}$ eV, and put $E_F = 0$ in the numerical calculations. The TMR at the angle $\theta$ is conventionally defined as

$$\mathrm{TMR}(\theta) = \frac{I(0) - I(\theta)}{I(0)}. \tag{15}$$

## III. MAGNETOTRANSPORT AT FINITE EXTERNAL MAGNETIC FIELDS

In the presence of a static external magnetic field, the description of the transport properties of electrons in a honeycomb lattice becomes much more involved due to the coupling between graphene and the electrodes associated with the Hofstadter problem. To circumvent this situation we describe the electrons in the honeycomb lattice as Dirac fermions in the continuum. At first we introduce the field operators[21,22]

$$\Psi_\sigma(\mathbf{r}) = \sum_q \frac{e^{iqx}}{\sqrt{L}}\begin{pmatrix} 0 \\ \phi_0(y) \end{pmatrix} d_{q\sigma} + \sum_{q,n,\alpha} \frac{e^{iqx}}{\sqrt{2L}}\begin{pmatrix} \phi_n(y - ql_B^2) \\ \phi_{n+1}(y - ql_B^2) \end{pmatrix} d_{qn\alpha\sigma}, \tag{16}$$

where $l_B = 1/\sqrt{eB}$ is the cyclotron length, $n = 0, 1, 2, \ldots$, $\alpha = \pm 1$, and $\phi_n(x)$ is the $n$th eigenfunction of the usual one-dimensional harmonic oscillator. The Hamiltonian describing the electrons in graphene acquires the second-quantized form

$$H_G = \sum_{qn\alpha\sigma} E(n,\alpha) d^\dagger_{qn\alpha\sigma} d_{qn\alpha\sigma}, \tag{17}$$

where

$$E(n,\alpha) = \alpha\omega_c\sqrt{n+1}$$

is the Landau level with $\omega_c = v_F\sqrt{2eB}$. The sum over integer $n$'s is cut off at $\mathcal{N}$. The coupling between graphene and ferromagnetic electrodes is

$$H_T = \sum_{kq\sigma} \phi_0(-ql_B^2)(T_{kLq}c^\dagger_{kL\sigma}d_{q\sigma} + T^*_{kLq}d^\dagger_{q\sigma}c_{kL\sigma}) + \sum_{kqn\alpha\sigma}[\phi_n(-ql_B^2) + \alpha\phi_{n+1}(-ql_B^2)][T_{kLq}c^\dagger_{kL\sigma}d_{qn\alpha\sigma} + T^*_{kLq}d^\dagger_{qn\alpha\sigma}c_{kL\sigma}]$$
$$+ \sum_{kq\sigma} \phi_0(L - ql_B^2)(T_{kRq}c^\dagger_{kR\sigma}d_{q\sigma} + T^*_{kRq}d^\dagger_{q\sigma}c_{kR\sigma}) + \sum_{kqn\alpha\sigma}[\phi_n(L - ql_B^2) + \alpha\phi_{n+1}(L - ql_B^2)][T_{kRq}c^\dagger_{kR\sigma}d_{qn\alpha\sigma} + T^*_{kRq}d^\dagger_{qn\alpha\sigma}c_{kR\sigma}], \tag{18}$$

where $L$ is length of graphene. Similar to the calculation of Eq. (11) we obtain the electrical current in the form

$$J_L = \frac{e}{\hbar}\int \frac{d\varepsilon}{2\pi}\mathrm{Tr}\{[\varepsilon - (1+\varepsilon X)\Sigma^r]^{-1}(1+\varepsilon X)^2 R\Gamma_R R^\dagger \times[\varepsilon - (1+\varepsilon X)\Sigma^a]^{-1}\Gamma_L\}[f_R(\varepsilon) - f_L(\varepsilon)], \quad (19)$$

where

$$X(\varepsilon) = \sum_{n\alpha}\frac{1}{\varepsilon - E(n,\alpha)} = \frac{2\varepsilon}{\omega_c^2}\left[\Psi\left(\frac{\omega_c^2-\varepsilon^2}{\omega_c^2}\right) - \Psi\left(\frac{(\mathcal{N}+2)\omega_c^2-\varepsilon^2}{\omega_c^2}\right)\right],$$

with $\Psi(z)$ denoting the digamma function.[23] The electric conductance can be obtained by $\partial J_L/\partial V$. For a small bias voltage we obtain the Landauer-Büttiker-type expression

$$G = \frac{e^2}{h}T_{\mathrm{eff}}, \quad (20)$$

where

$$T_{\mathrm{eff}} = \mathrm{Tr}\{\{E_F - [1+E_F X(E_F)]\Sigma^r\}^{-1}[1+E_F X(E_F)]^2 R\Gamma_R R^\dagger \times\{E_F - [1+E_F X(E_F)]\Sigma^a\}^{-1}\Gamma_L\}$$

plays the role of an effective energy-dependent transmission coefficient. In the limit $B\to 0$, we further obtain for $\theta=0$,

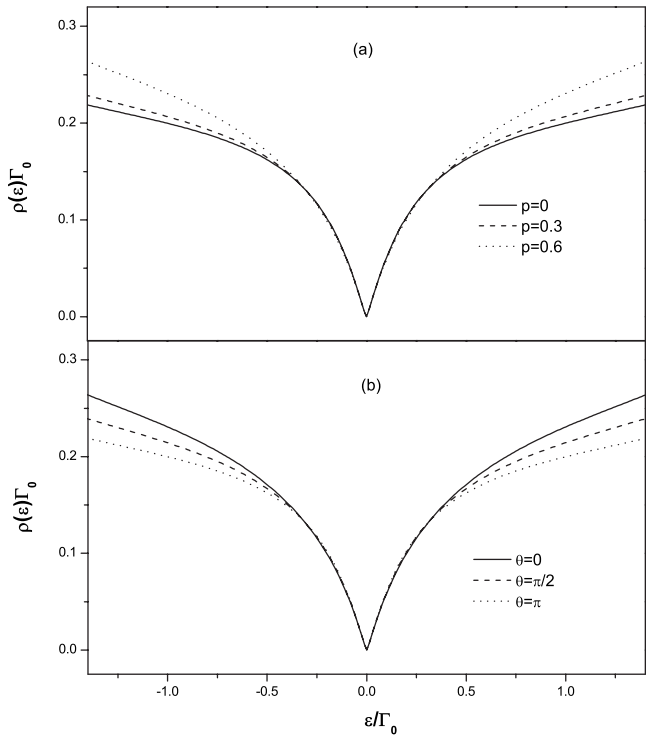


FIG. 2. DOS as a function of energy $\varepsilon$ for different polarization $p$ at (a) $\theta=0$ and for different angle $\theta$ at (b) $p=0.6$. The other parameters are taken as $D=2\Gamma_0$ and $B=0$.

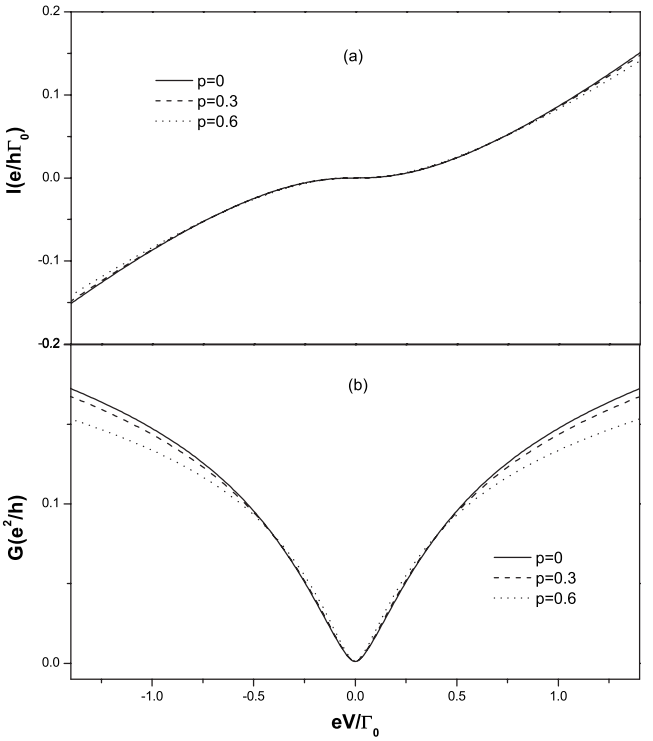


FIG. 3. The bias dependence of the electrical current $I$ (a) and differential conductance $G$ (b) for different polarization $p$ at $\theta=0$ and $k_BT=0.005\Gamma_0$. The other parameters are taken the same as those of Fig. 2.

$$T_{\mathrm{eff}} = \sum_\sigma \frac{\lambda\Gamma_L^\sigma\Gamma_R^\sigma}{E_F^2 + \frac{1}{4}\lambda(\Gamma_L^\sigma+\Gamma_R^\sigma)^2}, \quad (21)$$

where $\lambda = (2\mathcal{N}+3)^2 + 2(\mathcal{N}+1)(\mathcal{N}+2)(2\mathcal{N}+3)\frac{\omega_c^2}{E_F^2}$.

## IV. NUMERICAL RESULTS AND DISCUSSIONS

Adopting the wide bandwidth approximation for the graphene spin-valve system we neglect the energy dependence of the linewidth functions $\Gamma_\alpha^\sigma(\varepsilon)$. Denoting the spin polarization of the left and the right electrodes by, respectively, $p_L$ and $p_R$ we write $\Gamma_L^{\uparrow,\downarrow} = \Gamma_R^{\uparrow,\downarrow} = \Gamma_0(1\pm p)$; here $\Gamma_0$ describes the coupling between the graphene and the electrode without the internal magnetization. Here we assumed the left and the right electrodes to be of the same material. In the following numerical calculation, we take $\Gamma_0$ as the energy scale. We calculate the DOS in graphene via relation $\rho(\varepsilon) = -\frac{1}{\pi}\mathrm{Im}\Sigma_\sigma \mathcal{G}_a^{\sigma\sigma,r}(\varepsilon)$. Figure 2 shows the DOS as a function of energy for different polarization $p$ and magnetization angle $\theta$. It is clearly observed that the DOS displays a dip structure with the energy. For nonzero energy, the DOS increases with increasing $p$, however it decreases with increasing $\theta$. This is caused by the different tunneling rates for up and down spins owing to the splitting of DOS of the ferromagnetic leads. This splitting acts as an effective magnetic field[24] reaching values much larger than externally applied magnetic field.[25] This results in a spin dependence of the DOS in the central

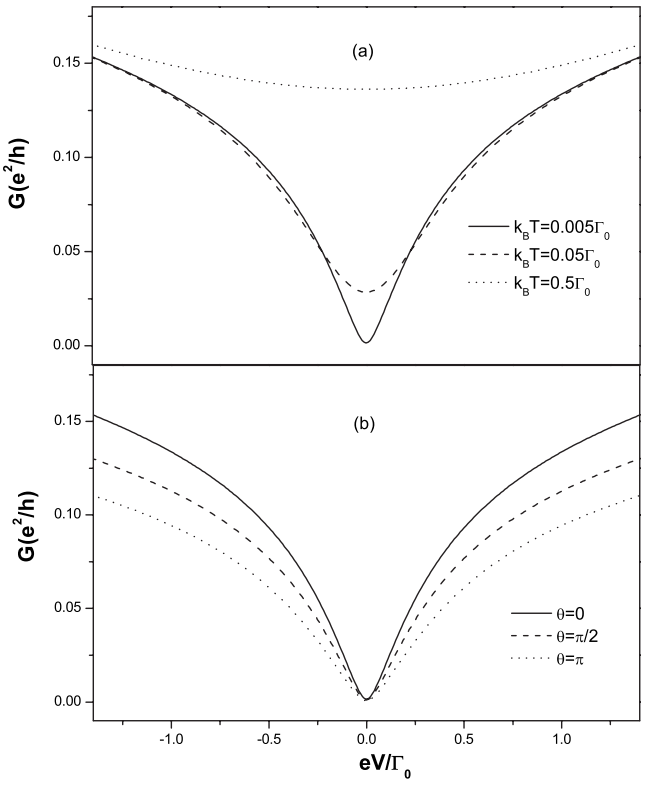


FIG. 4. The bias dependence of the differential conductance $G$ for different temperature $T$ at (a) $\theta=0$ and for different angle $\theta$ at (b) $k_BT=0.005\Gamma_0$. The parameters are taken the same as those of Fig. 2.

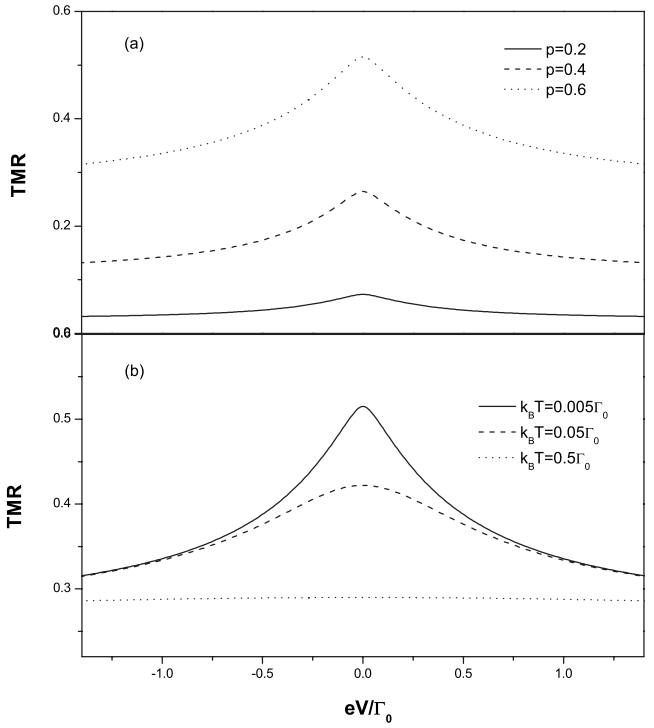


FIG. 5. The bias dependence of TMR for different polarization $p$ at (a) $k_BT=0.005\Gamma_0$ and for different temperature $T$ at (b) $p=0.6$. The other parameters are taken the same as those of Fig. 2.

region. While at the zero energy point, the DOS is independent of $p$ and $\theta$. This stems from the nature of Dirac point in the graphene.

The bias dependence of the electrical current and the differential conductance $G=dI/dV$ are shown in Fig. 3 for parallel electrodes magnetizations and for the different polarization $p$. The nonlinear behavior of $G$ and the strong dip at zero bias are in line with the experimental observations,[17] and are at variance with the typical behavior when a Fermi liquid is in central region instead of graphene. In that case the electrical current is proportional to the applied voltage at small bias and obeys the Ohmic law.[26] The results obtained here resemble rather the ferromagnet-insulator-ferromagnet (FM-I-FM) junctions.[27,28] The reason is that the DOS in graphene diminishes at the Fermi level. Hence, graphene sheet can be viewed as a tunneling barrier at the zero energy point, similar to FM-I-FM system. With increasing the polarization $p$, the portion of spin-up electron states increases while for the spin-down electrons it decreases. However, the scattering of the former is larger than that of the latter, thus we conclude that the conductance $G$ decreases with increasing $p$ at nonzero bias [cf. Fig. 3(b)]. While $G$ is almost independent of $p$ at zero bias, which stems from the fact that the spin transport through the Dirac point of graphene is ballistic due to its insulatorlike properties.

The bias dependence of the conductance at different temperatures $T$ and angles $\theta$ are shown in Fig. 4: the conductance is roughly independent of $T$ at large bias. Near $V=0$ the conductance increases with increasing $T$. This behavior is also in contrast to usual Fermi liquids where the conductance decreases with increasing temperature because thermal fluctuations enhance the scattering of conduction electrons and thereby contributes to the resistance of system.[26] In our case, the graphene is equivalent to a barrier at the zero energy point. Near zero-bias voltage, the thermally excited electrons are dominant in tunneling process. Therefore, with increasing temperatures, the increase in the thermally excited electrons enhances the conductance. On the other hand for large bias, the contributions to the conductance stem mainly from electrons with excess energies well above the Fermi level (as dictated by the applied voltage) which leads to a very weak dependence of the conductance on the temperature at large bias. The conductance as a function of $\theta$ [Fig. 4(b)] follows the conventional behavior of magnetic junctions such as the ferromagnet-quantum dot-ferromagnet system.[29–31] When $\theta$ changes from 0 to $\pi$ the number of spin-up and spin-down electrons is rearranged. Figure 5 shows TMR ratio as a function of the applied voltage for different polarizations $p$ and temperatures $T$. A pronounced cusplike feature appears at zero bias in line with experimental observations.[17] We assign this behavior to the result of a nontrivial combined effect of graphene and conventional spin-valve properties, evidenced by the dependence of TMR on the polarization $p$ at a fixed bias voltage [cf. Fig. 5(a)]. When increasing the polarization $p$ the contribution of spin-up states relative to the spin down is increased resulting in an increase in TMR for the entire bias range. However, the TMR changes in a nonlinear manner: the TMR value at zero bias becomes larger than that at nonzero bias. This is because for a small bias graphene be-

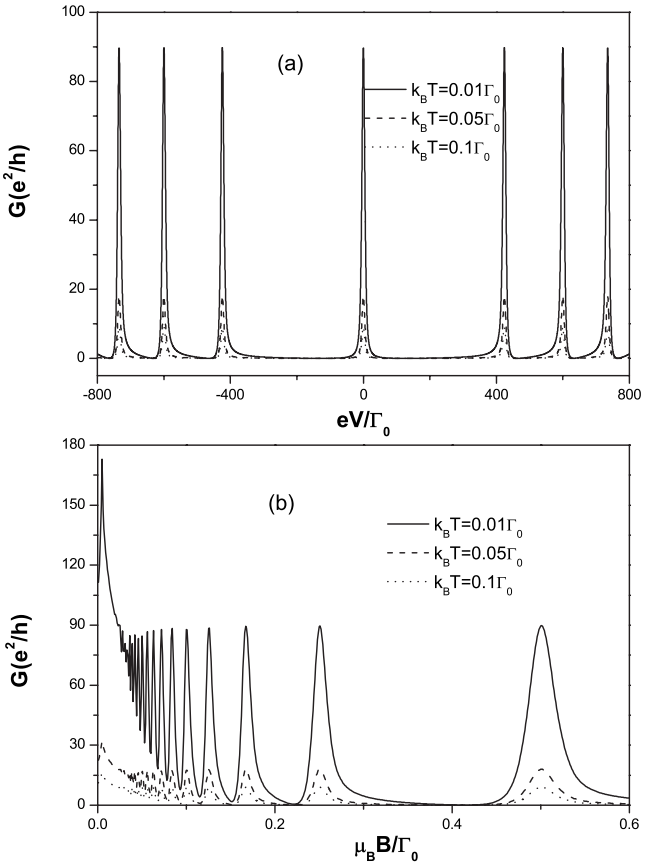


FIG. 6. The differential conductance as a function of the bias voltage at (a) $\mu_BB=1\Gamma_0$ and of the magnetic field at (b) $eV=300\Gamma_0$ for different temperature $T$ in the parallel configuration. The parameters are taken as $p=0.6$ and $\mathcal{N}=100$.

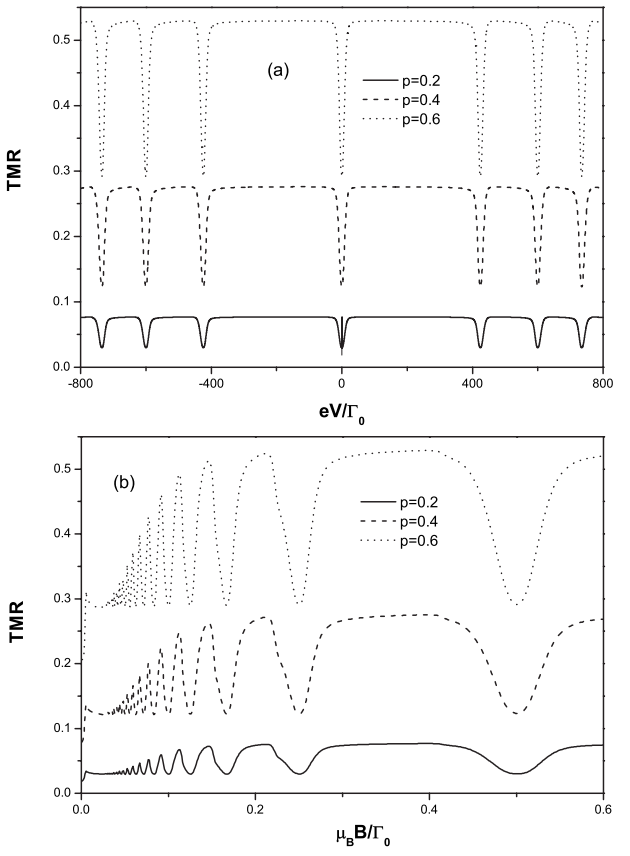


FIG. 7. The TMR as a function of the bias voltage at $\mu_BB=1\Gamma_0$ (a) and of the magnetic field at $eV=300\Gamma_0$ (b) for different polarization $p$ at $k_BT=0.1\Gamma_0$. The other parameters are taken the same as those of Fig. 6.

haves as an insulator. In contrast, for a large bias graphene behaves more like a metal, which is an essential difference between graphene and other materials in the central region. The spin tunneling is ballistic through an insulator in contrast to a metal, whence the TMR is more enhanced around zero bias. There are almost no changes with the temperature $T$ for large bias [see Fig. 5(b)]. With increasing temperatures more thermally excited electrons contribute to the electrical currents for the parallel and the antiparallel configurations; in fact, the increase in the electrical current is faster for the antiparallel configuration. Therefore, we can conclude that the TMR decreases at higher temperatures and the zero-bias anomaly diminishes in this situation.

The bias and the magnetic field dependencies of the differential conductance $G$ for the different temperatures in the parallel configuration of magnetization are shown in Fig. 6. $G$ versus the applied voltage exhibits an oscillating behavior. Each conductance peak corresponds to resonant transport through a Landau level. As bias voltage increases, the distance between two neighboring peaks decreases due to the decrease in the distance between neighboring Landau levels. The differential conductance oscillates as a function of the magnetic field, as shown in Fig. 6(b). This is due to resonant transport through the Landau levels at a particular magnetic field strength and the applied bias values. With increasing temperatures [Fig. 6(a)] the differential conductance decreases for all bias voltages. In particular, at zero bias the temperature dependence of the differential conductance is different from the magnetic field-free case. The explanation for these phenomena is as follows: the magnetic field lifts the insulator behavior at Dirac point in graphene, and thus thermal fluctuations suppress the conductance. Figure 7 shows the TMR as a function of the bias voltage and the magnetic field strength for different polarizations $p$. TMR reaches a minimal value at bias voltages corresponding to the conductance peaks and increases with increasing $p$ which is nothing but a spin-valve effect.

## V. SUMMARY

In conclusion, we have studied the spin-dependent transport through a graphene spin-valve device for a noncollinear configuration by means of Keldysh's nonequilibrium Green's function method. It is found that at a zero magnetic field, the current-voltage curves show a nonlinear behavior. The corresponding differential conductance exhibits a strong dip near zero bias. The TMR shows a zero-bias anomaly that depends on the leads' spin polarization. Increasing the bias TMR follows a behavior akin to a metallic or an insulating system depending on the value of the bias. In the presence of an external magnetic field, the differential conductance and TMR oscillate periodically due to a resonant transport

through Landau levels. At zero bias the differential conductance versus the temperature reveals a behavior different from the magnetic field-free case.

## ACKNOWLEDGMENTS

The work of K.H.D. was supported by the Natural Science Foundation of Hunan Province, China (Grant No. 08JJ4002), the National Natural Science Foundation of China (Grant No. 60771059) and Education Department of Hunan Province, China. J.B. and Z.H.Z. were supported by the cluster of excellence "Nanostructured Materials" of the state Saxony-Anhalt.

[1] K. S. Novoselov, A. K. Geim, S. V. Morozov, D. Jiang, Y. Zhang, S. V. Dubonos, I. V. Grigorieva, and A. A. Firsov, Science **306**, 666 (2004).
[2] K. S. Novoselov, D. Jiang, F. Schedin, T. J. Booth, V. V. Khotkevich, S. V. Morozov, and A. K. Geim, Proc. Natl. Acad. Sci. U.S.A. **102**, 10451 (2005).
[3] Y. Zhang, J. P. Small, M. E. S. Amori, and P. Kim, Phys. Rev. Lett. **94**, 176803 (2005).
[4] C. Berger, Z. Song, T. Li, X. Li, A. Y. Ogbazghi, R. Feng, Z. Dai, A. N. Marchenkov, E. H. Conrad, P. N. First, and W. A. de Heer, J. Phys. Chem. B **108**, 19912 (2004).
[5] J. McClure, Phys. Rev. **104**, 666 (1956).
[6] A. K. Geim and K. S. Novoselov, Nature Mater. **6**, 183 (2007).
[7] Y. Zhang, Y. W. Tan, H. L. Stormer, and P. Kim, Nature (London) **438**, 201 (2005).
[8] C. Berger, Z. Song, X. Li, X. Wu, N. Brown, C. Naud, D. Mayou, T. Li, J. Hass, A. N. Marchenkov, E. H. Conrad, P. N. First, and W. A. de Heer, Science **312**, 1191 (2006).
[9] D. Huertas-Hernando, F. Guinea, and A. Brataas, Phys. Rev. B **74**, 155426 (2006).
[10] C. L. Kane and E. J. Mele, Phys. Rev. Lett. **95**, 226801 (2005).
[11] Y. Yao, F. Ye, X. L. Qi, S. C. Zhang, and Z. Fang, Phys. Rev. B **75**, 041401(R) (2007).
[12] K. H. Ding, G. Zhou, Z. G. Zhu, and J. Berakdar, J. Phys.: Condens. Matter **20**, 345228 (2008).
[13] E. W. Hill, A. K. Geim, K. Novoselov, F. Schedin, and P. Black, IEEE Trans. Magn. **42**, 2694 (2006).
[14] N. Tombros, C. Jozsa, M. Popinciue, H. T. Jonkman, and B. J. Van Wees, Nature (London) **448**, 571 (2007).
[15] S. Cho, Yung-Fu Chen, and M. S. Fuhrer, Appl. Phys. Lett. **91**, 123105 (2007).
[16] M. Ohishi, M. Shiraishi, R. Nouchi, T. Nozaki, T. Shinjo, and Y. Suzuki, Jpn. J. Appl. Phys., Part 1 **46**, L605 (2007).
[17] W. H. Wang, K. Pi, Y. Li, Y. F. Chiang, P. Wei, J. Shi, and R. K. Kawakami, Phys. Rev. B **77**, 020402(R)(2008).
[18] H. Haug and A. P. Jauho, *Quantum Kinetics in Transport and Optics of Semiconductors* (Springer, Berlin, 1998).
[19] V. P. Gusynin and S. G. Sharapov, Phys. Rev. B **73**, 245411 (2006).
[20] A. H. Castro Neto, F. Guinea, N. M. R. Peres, K. S. Novoselov, and A. K. Geim, arXiv:0709.1163, Rev. Mod. Phys. (to be published).
[21] N. M. R. Peres, F. Guinea, and A. H. Castro Neto, Phys. Rev. B **73**, 125411 (2006).
[22] B. Dóra and P. Thalmeier, Phys. Rev. B **76**, 035402 (2007).
[23] *Handbook of Mathematical Functions*, edited by M. Abramowitz and I. A. Stegun (Dover, New York, 1968).
[24] Z. G. Zhu, Phys. Lett. A **372**, 695 (2008).
[25] A. N. Pasupathy *et al.*, Science **306**, 86 (2004).
[26] H. F. Mu, G. Su, Q. R. Zheng, and B. Jin, Phys. Rev. B **71**, 064412 (2005).
[27] J. S. Moodera, Lisa R. Kinder, T. M. Wong, and R. Meservey, Phys. Rev. Lett. **74**, 3273 (1995).
[28] J. S. Moodera, J. Nowak, and Rene J. M. van de Veerdonk, Phys. Rev. Lett. **80**, 2941 (1998).
[29] N. Sergueev, Qing-Feng Sun, Hong Guo, B. G. Wang, and J. Wang, Phys. Rev. B **65**, 165303 (2002).
[30] H.-F. Mu, G. Su, and Q.-R. Zheng, Phys. Rev. B **73**, 054414 (2006).
[31] Z.-G. Zhu, G. Su, Q.-R. Zheng, and B. Jin, Phys. Rev. B **70**, 174403 (2004).